ADVANCED THEORY AND SIMULATIONS
www.advtheorysimul.com

Analytical Model of the Piezoresistive Behavior of Highly Compressible Sensors Made of Microporous Nanocomposites

*Jianpeng Zhang, Ziya Wang, and Zhengchun Peng**

Microporous conductive nanocomposites, compared with conventional filler-matrix composites, enable flexible piezoresistive sensors with higher sensitivity and a larger measurement range. Previous research focuses on different methods of fabricating porous materials that are highly sensitive to pressure, however, there is only a small amount of research studying the mechanism of those sensors. Without an appropriate theoretical guide, relying on expensive experimental approaches to enhance the sensitivity will significantly limit the advancement of this technology. This article proposes an efficient analytical model, with some parameters determined from experiments, to investigate the piezoresistive behaviors of microporous nanocomposites. The predicted results agree well with the analysis from finite element models as well as the experimental data. Moreover, scaling law is applied to study the effect of geometry, material, and interface on the sensitivity of the sensor. This study establishes the theoretical foundation for the design of a high-performance piezoresistive sensor based on microporous nanocomposites.

1. Introduction

Owing to their charismatic properties, such as the effective elastic modulus and bending stiffness, are close to those of human skin, soft piezoresistive sensors have attracted many researchers.[1–3] These sensors have many potential applications, including electronic skin for robots and prosthesis, epidermal electronics for human health monitor, and human-machine interface devices.[4–7] Conductive polymers, including conductive organic composites, ionic hydrogels and inorganic composite doped with conductive fillers, have been employed to fabricate soft piezoresistive sensors with high stretchability.[8–10] A wide conductivity range of doped nanocomposites has been achieved via fillers like metal nanoparticles, carbon black (CB), carbon nanotubes (CNT), and graphene, in order to meeting the requirement of different applications.[11–13] In addition, a variety of microstructured conductive nanocomposites are proposed to further improve their sensitivity and increase their measurement range to pressure.[14] For instance, Tang et al.[15] introduced a multi-layered flexible pressure sensor with microstructured polydimethylsiloxane (PDMS) films doped with reduced oxide graphene to provide an ultrahigh sensitivity over a wide pressure-range (2.5–1051 kPa^{-1} and 0.01–400 kPa). Wang et al.[16] employed a full 3D printing process to fabricate a hierarchically porous sensor with high sensitivity, good stretchability, and excellent durability. Guan et al.[17] adopted a bioinspired strategy to make a piezoresistive sensor with a graded porous structure, which exhibited ultra-wide measurement range, remarkable mechanical stability, and adequate sensitivity. These researches proposed many advanced fabrication processes for highly sensitive microporous nanocomposites. However, the rational structural design and subtle engineering of the material properties were based on a significant amount of experiment, which required major expenditure on costly equipment and time.

Up to date, three design strategies have been utilized in order to realizing highly sensitive sensors. First, intrinsic piezoresistive materials with high gauge factor (the specific value of resistance variation against strain), such as silicon film and carbon film, were used.[18,19] Although the GF of these materials can reach more than 2000, sensors made of these materials can only apply to small-strain environments due to the fragility of the materials.[20] Another avenue is to introduce microstructures, such as pyramid,[21] in the piezoresistive sensors to enhance the change of electrical contact resistance (ECR). When pressing on these sensors, contact area would drastically increase, leading to large reduction of ECR. In this approach, concentrated strain at contact tips would occur, which compromise the durability.[22] A pragmatic design of piezoresistive sensors utilizes the structural deformation of microporous nanocomposites, which causes the change of effective resistivity.[15] Efficiently coupling the changes

J. Zhang, Z. Peng
Key Laboratory of Optoelectronic Devices and Systems of Ministry of Education, College of Physics and Optoelectronic Engineering
Shenzhen University
Shenzhen 518060, China
E-mail: zcpeng@szu.edu.cn
Z. Wang
Shenzhen Institute of Artificial Intelligence and Robotics for Society (AIRS)
Shenzhen 518129, China

The ORCID identification number(s) for the author(s) of this article can be found under https://doi.org/10.1002/adts.202100247

DOI: 10.1002/adts.202100247

of resistivity and geometry of the sensor, this method is highly effective according to following equation:[23]

$$\Delta R/R = \Delta\rho/\rho + (1+2\nu)\,\Delta l/l \tag{1}$$

where $R$and ρ are the resistance and resistivity, l andμ are the effective length and Poisson's rate, respectively. Also, conducting behavior of porous media in petrophysics is an important factor for analyzing the reservoir characteristics, and the research on this topic is very mature. However, this conclusive formula is insufficient to guide the design of such sensor. Till now, there are few appropriate analytical models to describe the specific piezoresistive behaviors of microporous nanocomposites.

In this work, we propose an analytical model to study the piezoresistive mechanism of a sensor made of microporous nanocomposites. An open-cell microporous nanocomposite composed of carbon black (CB)/ thermoplastic polyurethane (TPU) is used as an example. Considering relevant studies with high recognition, the Stroker's model of compressed material[24] and quantum tunnelling theory of porous medias[25] are employed to study the piezoresistive response of the sensor. With the lumpy interface between the microporous nanocomposite and the metal electrodes, the ECR can be not ignored. As such, a previously reported analytical model[26] is integrated in our study. The prediction of the piezoresistive behavior of the microporous CB/TPU sensor by our integrated analytical model is validated by FEA results. Furthermore, microporous nanocomposites with different porosities and CB contents are studied by experiments to validate the accuracy of the analytical model. In addition, scaling law[27] is used to study the effect of the geometry of sensing layer, the layout and dimension of the interdigitated electrodes, and the contact condition between the sensing layer and the electrodes on the sensitivity of the sensor to pressure.

2. Analytical Approach

2.1. Mechanical Model of Microporous Solids

Highly porous materials are well-known representatives of the compressible solid.[28] Constriction of these materials and collapse of their pore structures would happen when their loading pressures are larger than their yield stress.[24] In order to describe the hyper-elastic behavior of highly compressible solids, one of the most accepted models is the modified Ogden model in which a compressible energy term is added to the Ogden's incompressible hyper-elastic model.[29,30] After further developments, the highly compressible hyper-elastic model is implemented in Abaqus[31] based on the work of Storakers, which can be expressed as:

$$W\left(\lambda_1,\lambda_2,\lambda_3\right) = \sum_{i=1}^{n} \frac{2\mu_i}{\alpha_i^2}\left[\lambda_1^{\alpha_i} + \lambda_2^{\alpha_i} + \lambda_3^{\alpha_i} - 3 + \frac{1}{\beta_i}\left(J^{-\alpha_i\beta_i} - 1\right)\right] \tag{2}$$

where W is the strain energy density, $\lambda_i(i=1,2,3)$is primary elongation, $n$is the order of the model, J is the volume ratio, and α_i, β_i, and μ_i $(i=1,2,3)$are material parameters. Furthermore, the initial shear(μ_0)and bulk modulus(K_0)of the material can be written as:

$$\mu_0 = \sum_{i=1}^{n}\mu_i > 0 \quad K_0 = \sum_{i=1}^{n} 2\mu_i\left(\beta_i + \frac{1}{3}\right) > 0 \tag{3}$$

which means that$\mu_0$and K_0have positive values. According to the strain energy density function in Equation (2), the principal stresses can be obtained as:

$$\sigma_k = \lambda_k\frac{\partial W}{\partial\lambda_k} = \frac{1}{\lambda_k}\sum_{i=1}^{n}\frac{2\mu_i}{\alpha_i}\left(\lambda_k^{\alpha_i} - J^{-\alpha_i\beta_i}\right)(k=1,2,3) \tag{4}$$

Given that the transversal deformations of microporous materials can be ignored, which gives $\beta_i \approx 0, (i=1,2,3)$, So the principal stresses can be simplified as:

$$\sigma = \frac{1}{\lambda}\sum_{i=1}^{n}\frac{2\mu_i}{\alpha_i}\left(\lambda^{\alpha_i} - 1\right) \tag{5}$$

Highly compressible behaviors of the microporous material correspond with the highly compressible hyper-elastic model, whose transversal deformations can be ignored ($\nu \approx 0$).[32] Therefore, the deformation rate of the microporous material is approximate positive correlation with its porosity η, which can be written as:

$$\eta = 1 - \lambda\left(1 - \eta_0\right) \tag{6}$$

where η_0 is the original porosity. Then, the relational expression of the principal stresses and porosity η can be approximately expressed as:

$$\sigma = \frac{1}{\lambda}\sum_{i=1}^{n}\frac{2\mu_i}{\alpha_i}\left(\frac{1-\eta}{1-\eta_0}\right)^{\alpha_i}\left[\lambda^{\alpha_i} - 1\right] \tag{7}$$

2.2. Electrical Model of Microporous Solids

When the microporous material is compressed, the reduction of its volume would yield a smaller porosity and a denser conductive network. The increase of interconnected conducting routes inside the material reduces its resistance. Based on Archie's empirical model describing the relational expression of electrical conductivity and porosity of sand,[33] the electrical model of microporous conductive material is performed. The conducting routes of microporous conductive material are similar with those of sand due to the same depositional fabric between sandstone in water and pore-forming inorganic salt, such as NaCl, in the precursor mixture. Considering that the definition of porosity$\eta$is complementary between sand and microporous conductive material, the empirical electrical model of microporous conductive material can be converted as:

$$\kappa = \kappa_0(1-\eta)^m \tag{8}$$

where κ and κ_0 are the conductivity of the porous material and non-porous basis materials and m is cementation exponent depended on the microcellular structures. According to a quantitative general effective media (GEM) theory[34] and Equation (6),

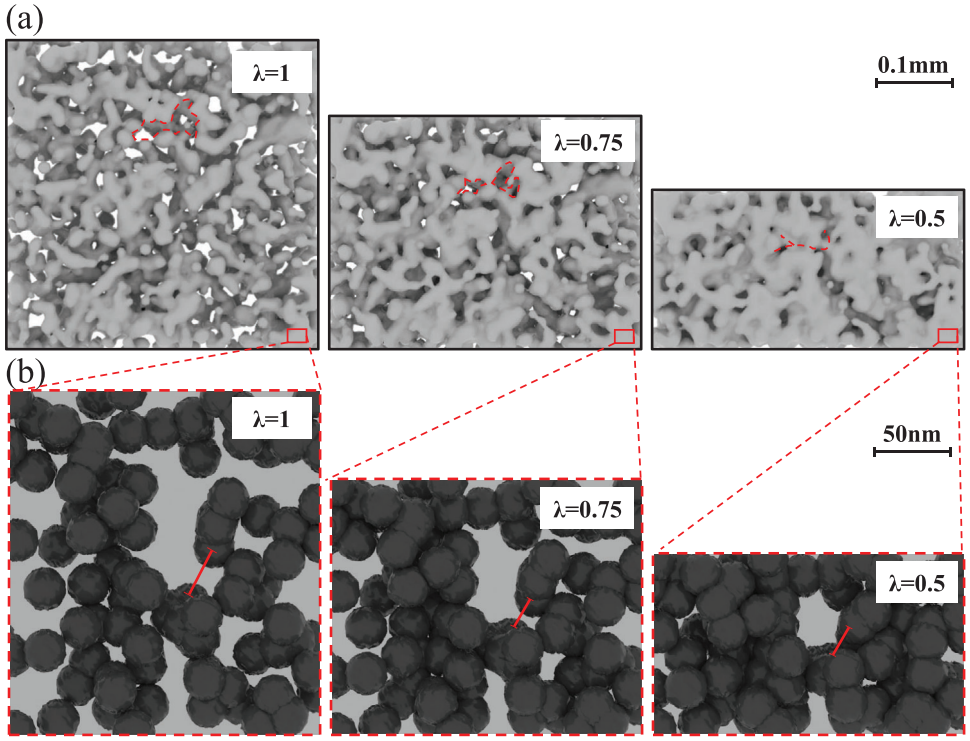

Figure 1. Closure of internal pores (a) and the reduction of the distances between doped CB clusters (b) in microporous nanocomposites by pressing.

the relational expression of porosity$\eta$and elongation λcan be obtained as:

$$\kappa = \kappa_0 \frac{(1-\eta_0)^m}{\lambda^m} \tag{9}$$

When the microporous conductive material contains conductive fillers, such as CB clusters in CB/TPU composites, its microcosmic deformation behaviors are shown in **Figure 1**. The decrease of the distance between each doped CB cluster reveals that the quantum tunnelling effects are not negligible.[14,34] Therefore, a modified electrical model is proposed by adding a term describing the quantum tunnelling effects, which can be written as:

$$\kappa = \kappa_0 \frac{(1-\eta)^m}{\lambda^a} \tag{10}$$

where a is quantitative coefficient depended on the microcellular structures, conductive fillers, and substrate material.

2.3. Electrical Contact Resistance (ECR) at Microporous Interface

Due to the increase of contact areas during compressing the sensor, the increase of conductive routes also exists at microporous interface between microporous materials and electrodes. Traditional quantitative ECR theory integrating the equivalent contact radius (r_{eq}) can be written as:

$$R_{cr} = \frac{\rho_E + \rho_S}{4r_{eq}} \tag{11}$$

where R_{cr} is ECR, $\rho_S$and ρ_E are the resistivity of sensing layer and electrode, and $r_{eq} = \sqrt{A_{eq}/\pi}$ andA_{eq} is equivalent contact area. According to the general effective media (GEM) theory, the equivalent contact area A_{eq} is inversely proportionate to $1-\eta$, as shown in **Figure 2**. Then, taking quantum tunnelling effects, micro-nanostructures, and Equation (6) into consideration,[26] the equivalent contact area can be modified as:

$$A_{eq} = \frac{A_{eq0}}{\lambda^{2b}(1-\eta)} \tag{12}$$

with A_{eq0} as original equivalent contact area and b as contact-strain correlation index. The resistivity of electrode is far smaller than that of carbon-rubber systems and can be ignored, so that the ECR can be obtained as:

$$R_{cr} = \frac{\sqrt{\pi}\lambda^{a+b}}{4\kappa_0(1-\eta)^{m-0.5}\sqrt{A_{ged}dW}} \tag{13}$$

with A_{eq0}=$A_{ged}dW$, in which A_{ged} is effective contact area per unit area, and$d$and W are the thickness and width of electrodes, respectively.

2.4. Analytical Model of Microporous Pressure Sensor with a Pair of Electrodes

Figure 3a shows a simple 3D model of piezoresistive sensor consisting of a microporous sensing layer and a pair of electrodes, which form an electrical loop. The distribution of potential in the

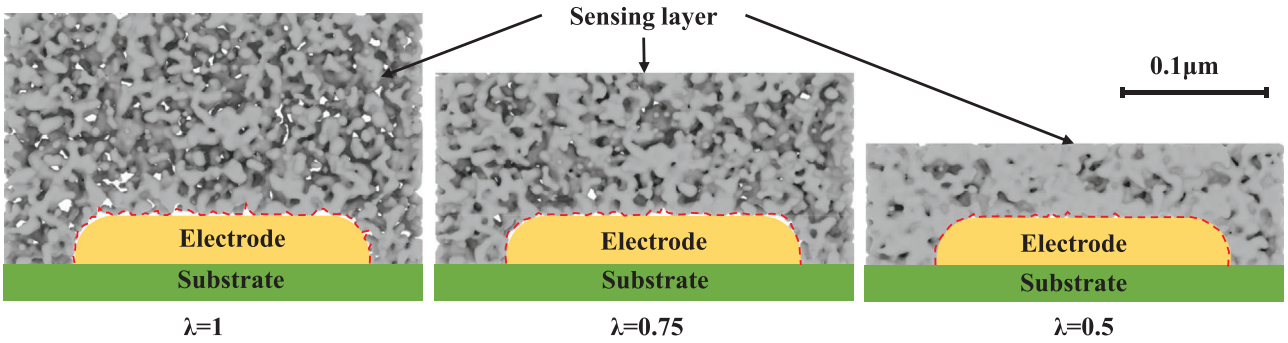

Figure 2. The change of effective ECR at the microporous interface by pressing.

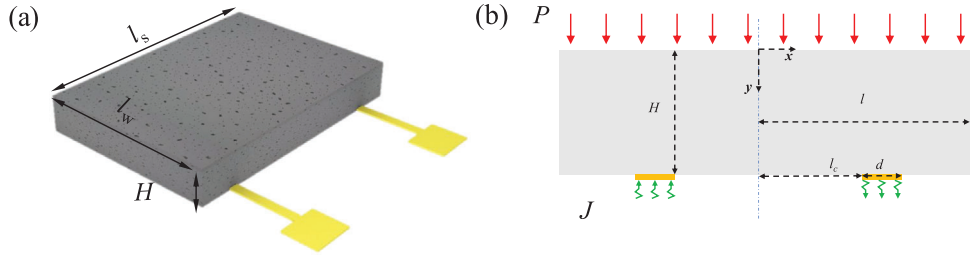

Figure 3. a) Schematic exploded view of a pressure sensor. b) Simplified 2D analytical model of the sensor.

sensing layer can be described by Laplace's equation for the electrostatic field as:

$$\frac{\partial^2 E}{\partial x^2} + \frac{\partial^2 E}{\partial y^2} + \frac{\partial^2 E}{\partial z^2} = 0 \tag{14}$$

with E as potential and (x, y, z) as spatial coordinates. Because the equipotential line is consistent along z-coordinate, the 3D model can be simplified as 2D as shown in Figure 3b. Thus, the governing equation can be written as:

$$\frac{\partial^2 E}{\partial x^2} + \frac{\partial^2 E}{\partial y^2} = 0 \tag{15}$$

By applying variable separating solution methods, the solution of E can be written as:

$$E = \Phi(x)\,\Gamma(y) \tag{16}$$

If the symmetric plane of sensing layer is defined as zero-potential surface, antisymmetric relations $E(-x, y) = -E(x, y)$ and boundary condition $\partial E/\partial x|_{x=l} = 0$ give eigen equation $\phi(x)$ of $\Phi(x)$ as:

$$\phi_i(x) = sin\left(\beta_i x\right) \tag{17}$$

with $\beta_i = (2i+1)\pi/2l, (i = 0, 1, 2\ldots)$ and $2l$ as the length of sensor. Then, the solution of E can be obtained as:

$$E = \sum_{i=0}^{\infty} \left[A_i \cosh\left(\beta_i y\right) + B_i \sinh\left(\beta_i y\right)\right] \sin\left(\beta_i x\right) \tag{18}$$

where A_i and B_i are underdetermined coefficient depended on boundary conditions. According to simplified model, the boundary condition can be expressed as:

$$\kappa \left.\frac{\partial E}{\partial y}\right|_{y=0} = 0 \;\kappa \left.\frac{\partial E}{\partial y}\right|_{y=H} = \begin{cases} J, l_c \le x \le l_c + d \\ 0, \text{other} \end{cases} \tag{19}$$

with H, d, and l_c as thickness of sensing layer, width, and position of electrode, and J as equivalent average current density, respectively. The confirmed solution of E can be obtained as:

$$E = \sum_{i=0}^{\infty} \frac{4J \sin\left(\frac{\beta_i d}{2}\right) \sin\left[\beta_i\left(l_c + \frac{d}{2}\right)\right]}{\kappa l \beta_i^2 sinh\left(\beta_i H\right)} \cosh\left(\beta_i y\right) sin\left(\beta_i x\right) \tag{20}$$

Based on the above solutions, the equivalent average potential at the location of electrode can be calculated as:

$$\overline{E} = \frac{1}{d}\int_{l_c}^{l_c+d} E dx = \sum_{i=0}^{\infty} \frac{8J \sin^2\left(\frac{\beta_i d}{2}\right) \sin^2\left[\beta_i\left(l_c + \frac{d}{2}\right)\right]}{\kappa l d \beta_i^3 tanh\left(\beta_i H\right)} \tag{21}$$

Therefore, the equivalent resistance between a pair of electrodes can be obtained as:

$$R_s = \frac{2\overline{E}}{JaW} = \sum_{i=0}^{\infty} \frac{16 \sin^2\left(\frac{\beta_i d}{2}\right) \sin^2\left[\beta_i\left(l_c + \frac{d}{2}\right)\right]}{\kappa l W d^2 \beta_i^3 tanh\left(\beta_i H\right)} \tag{22}$$

Taking the compressibility of microporous nanocomposite into consideration, the change of length l can be ignored and the change of thickness can be written as λH. Combining with

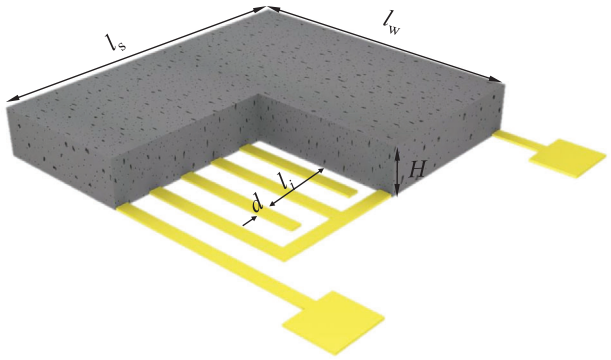

Figure 4. A pressure sensor coupling with an interdigitated electrode.

Equations (10) and (22), the equivalent resistance changing with compressed deformation can be obtained as:

$$R_s = \sum_{i=0}^{\infty} \frac{16\lambda^a \sin^2\left(\frac{\beta_i d}{2}\right) \sin^2\left[\beta_i\left(l_c + \frac{d}{2}\right)\right]}{\kappa_0(1-\eta)^m l W d^2 \beta_i^3 tanh\left(\beta_i \lambda H\right)} \tag{23}$$

2.5. Analytical Model of Microporous Pressure Sensors with an Interdigitated Electrode

Figure 4 shows a microporous pressure sensor with an interdigitated electrode integrated with sensing layer. Based on linear superposition principle, the potential distribution approximately equals the superposition of many pairs of electrodes, which yields:

$$E = \sum_{i=0}^{\infty} \frac{4\sin\left(\frac{\beta_i d}{2}\right) \sum_{n=1}^{N} (-1)^{n-1} J_n \sin\left[\beta_i\left(l_n + \frac{d}{2}\right)\right]}{\kappa l \beta_i^2 sinh\left(\beta_i H\right)} \times \cosh\left(\beta_i y\right) sin\left(\beta_i x\right) \tag{24}$$

with N as the number of pairs. Combined with Equation (21), the potential of electrodes can be obtained as:

$$\overline{E}_j = \frac{1}{d}\int_{l_j}^{l_j+d} E dx = \sum_{i=0}^{\infty} \frac{8\sin^2\left(\frac{\beta_i d}{2}\right) \sin\left[\beta_i\left(l_j + \frac{d}{2}\right)\right] \left\{\sum_{n=1}^{N} J_n \sin\left[\beta_i\left(l_n + \frac{d}{2}\right)\right]\right\}}{\kappa l d \beta_i^3 tanh\left(\beta_i H\right)} \tag{25}$$

Taking the compressed deformation into consideration, the equation set can be transformed as:

$$\mathbf{E} = [C]_{N\times N}\mathbf{J} \tag{26}$$

where $[C]_{N\times N}$ is the conductance matrix with:

$$\mathbf{E} = [\,\bar{E}_1\ \bar{E}_2\ \cdots\ \bar{E}_n\,]^{\mathrm{T}} \quad \mathbf{J} = [J_1\ J_2\ \cdots\ J_n\,]^{\mathrm{T}} \tag{27}$$

$$c_{nk} = \sum_{i=0}^{\infty} \frac{8\lambda^a \sin^2\left(\frac{\beta_i d}{2}\right) \sin\left[\beta_i\left(l_n + \frac{d}{2}\right)\right] \sin\left[\beta_i\left(l_k + \frac{d}{2}\right)\right]}{\kappa_0(1-\eta)^m l d \beta_i^3 tanh\left(\beta_i \lambda H\right)} \tag{28}$$

Because the conductivity of electrode is far larger than that of sensing layer, the potential of electrode satisfies the relational expression as:

$$\bar{E}_1 = -\bar{E}_2 = \cdots = (-1)^{n-1}\bar{E}_n = E_{eq} \tag{29}$$

Hence, Equation (26) can be written as:

$$\mathbf{J} = E_{eq}[C]_{N\times N}^{-1}\mathbf{a} \tag{30}$$

with:

$$\mathbf{a} = \left[\,1\ -1\ \cdots\ (-1)^{n-1}\,\right]_N^{\mathrm{T}} \tag{31}$$

Combined with Equation (30), the effective resistance yields:

$$R_s = \frac{2E_{eq}}{\left[\sum_{n=1}^{N}(-1)^{n-1}J_n\right] dW} = \frac{2}{dW\mathbf{a}^{\mathrm{T}}[C]_{N\times N}^{-1}\mathbf{a}} \tag{32}$$

The total resistance, coupled with ECR, can be obtained as:

$$R = R_s + 2R_{cr}/N = \frac{2}{dW\mathbf{a}^{\mathrm{T}}[C_{N\times N}]^{-1}\mathbf{a}} + \frac{\sqrt{\pi}\lambda^{a+b}}{2N\kappa_0(1-\eta)^{m-0.5}\sqrt{A_{ged}dW}} \tag{33}$$

2.6. Scaling Law for the Design of Microporous Pressure Sensor

Taking the simple model in Figure 2 as an example, the total resistance of the sensor can be obtained as:

$$R = R_s + 2R_{cr} = \sum_{i=0}^{\infty} \frac{16\lambda^a \sin^2\left(\frac{\beta_i d}{2}\right) \sin^2\left[\beta_i\left(l_c + \frac{d}{2}\right)\right]}{\kappa_0\left(1-\eta_m\right)^m l d^2 \beta_i^3 tanh\left(\beta_i \lambda H\right) W} + \frac{\sqrt{\pi}\lambda^{a+b}}{2\kappa_0(1-\eta)^{m-0.5}\sqrt{A_{ged}dW}} \tag{34}$$

A key parameter for designing a pressure sensor is sensitivity to pressure or deformation. The sensitivity equals the specific value of resistance against original resistance, which yields:

$$s = \frac{R}{R_0} = \frac{\sum_{i=0}^{\infty} \frac{16\lambda^a \sin^2\left(\frac{\beta_i d}{2}\right)\sin^2\left[\beta_i\left(l_c+\frac{d}{2}\right)\right]}{l d^2 \beta_i^3 tanh\left(\beta_i \lambda H\right)} + \frac{\sqrt{\pi(1-\eta)W}\lambda^{a+b}}{2\sqrt{A_{ged}d}}}{\sum_{i=0}^{\infty} \frac{16\sin^2\left(\frac{\beta_i d}{2}\right)\sin^2\left[\beta_i\left(l_c+\frac{d}{2}\right)\right]}{l d^2 \beta_i^3 tanh\left(\beta_i H\right)} + \frac{\sqrt{\pi(1-\eta)W}}{2\sqrt{A_{ged}d}}} \tag{35}$$

By mean of scaling law methods, this equation can be simplified to:

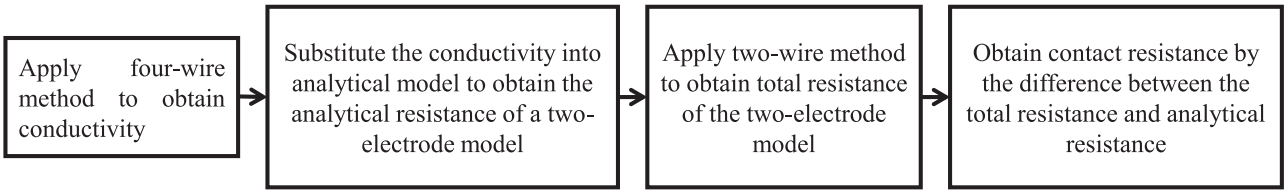

Figure 5. The experimental procedure of characterizing total resistance and ECR.

$$s = \frac{\sum_{i=0}^{\infty} \Pi\left(\frac{l_c}{l}, \frac{d}{l}, i\right) \coth\left(\frac{2i+1}{2}\pi\lambda\left(\frac{H}{l}\right)\right) \lambda^a + \Psi\left(\frac{d}{l}, \frac{W}{l}, \eta, A_{ged}\right) \lambda^{a+b}}{\sum_{i=0}^{\infty} \Pi\left(\frac{l_c}{l}, \frac{d}{l}, i\right) \coth\left(\frac{2i+1}{2}\pi\left(\frac{H}{l}\right)\right) + \Psi\left(\frac{d}{l}, \frac{W}{l}, \eta, A_{ged}\right)} \tag{36}$$

with:

$$\Pi\left(\frac{l_c}{l}, \frac{d}{l}, i\right) = \frac{16\sin^2\left(\frac{2i+1}{4}\pi\left(\frac{d}{l}\right)\right)\sin^2\left[\frac{2i+1}{2}\pi\left(\left(\frac{l_c}{l}\right) + \frac{1}{2}\left(\frac{d}{l}\right)\right)\right]}{\left(\frac{d}{l}\right)^2\left(\frac{2i+1}{2}\pi\right)^3} \tag{37}$$

$$\Psi\left(\frac{d}{l}, \frac{W}{l}, \eta, A_{ged}\right) = \frac{\sqrt{\pi(1-\eta)\left(\frac{W}{l}\right)}}{2\sqrt{A_{ged}\left(\frac{d}{l}\right)}} \tag{38}$$

Sensitivities to deformation (D_S) and pressure (D_P) can be obtained at original position of a microporous pressure sensor and can be written as:

$$D_S = \left.\frac{ds}{d\lambda}\right|_{\lambda=1} = a + \frac{\left[\begin{array}{l} b\Psi\left(\frac{d}{l}, \frac{W}{l}, \eta, A_{ged}\right) \\ -\sum_{i=0}^{\infty} \Pi\left(\frac{l_c}{l}, \frac{d}{l}, i\right)\left(\frac{2i+1}{2}\pi\left(\frac{H}{l}\right)\right)\mathrm{csch}^2\left(\frac{2i+1}{2}\pi\left(\frac{H}{l}\right)\right) \end{array}\right]}{\sum_{i=0}^{\infty} \Pi\left(\frac{l_c}{l}, \frac{d}{l}, i\right) \coth\left(\frac{2i+1}{2}\pi\left(\frac{H}{l}\right)\right) + \Psi\left(\frac{d}{l}, \frac{W}{l}, \eta, A_{ged}\right)} \tag{39}$$

$$D_P = \frac{ds}{d\sigma} = \left.\frac{ds}{d\lambda}\right/\left.\frac{d\sigma}{d\lambda}\right|_{\lambda=1} = D_s \Big/ \sum_{i=1}^{n} 2\mu_i \tag{40}$$

3. Fabrication and Measurement

3.1. Fabrication of Microporous CB/TPU Nanocomposites

In this paper, microporous CB/TPU nanocomposite is taken as an example to study the piezoresistive behaviors of microporous nanocomposite. Its fabrication depending on the salting out method is as follows. First, a precursor solution was prepared by dissolving TPU particles into *N,N*-dimethylformamide (DMF, Aladdin) solvent. NaCl microparticles and CB nanoparticles (SUPER P Li, TIMCAL, and EC300J, Ketjenblack) were mixed with the precursor to act as a sacrificial template and an electrical filler, respectively. The NaCl microparticles (≈30 μm) was obtained by using planetary ball milling (F-P400, FOCUCY) and the CB nanoparticles was dispersed into ethyl acetate (EAC) solvent (99.5%, Aladdin) under sonication (JY92-IIDN, SCIENTZ) to enhance the dispersion uniformity. Then, the mixture was stirred by a double-blade planetary vacuum mixer (HM800, HASAI) and evenly coated on a glass plate. After that, thermally processed to remove organic solvent (DMF and EAC) was applied to solidify the slurry. Finally, NaCl microparticles were entirely dissolved by immersing the nanocomposites in water to create micropores.

3.2. Experimental Procedure

A field emission scanning electron microscope (SEM) (Supra 55, ZEISS) and an optical metallographic microscope (TM3030, Hitachi) were used to observe the microstructures of microporous CB/TPU nanocomposites. A measuring system combining a universal material testing machine (E1000, Instron) and a digital multimeter (34465A, Keysight) was set up to obtain a resistance–deformation and stress–deformation relational expression. According to the experimental procedure shown in **Figure 5**, conductivity, ECR, and total resistance of sensors were obtained in turn. First, the conductivity was measured by a four-wire method and the total resistance was measured by a two-wire method. Then, according to the above analytical model and experimental results, the ECR can be calculated.

3.3. Finite Element Analysis (FEA) of Piezoresistive Behaviors

3D FEA models were established to simulate piezoresistive behaviors of microporous pressure sensors and to verify the accuracy and reasonableness of analytical models. Because of the similarity between thermal governing equations and electrical governing equations, Static thermomechanical modules in ABAQUS software were applied to simulate electromechanical behaviors. The relation between conductivity and strain of microporous CB/TPU nanocomposites was defined by UMAT subprogram as in Appendix. The conducting elements are defined as:

$$COND = \kappa_0(1-\eta)^m \tag{41}$$

$$FLUX = -COND \times DTEMDX \times (1+NE)^a \tag{42}$$

$$DFDG = -COND \times (1+NE)^a \tag{43}$$

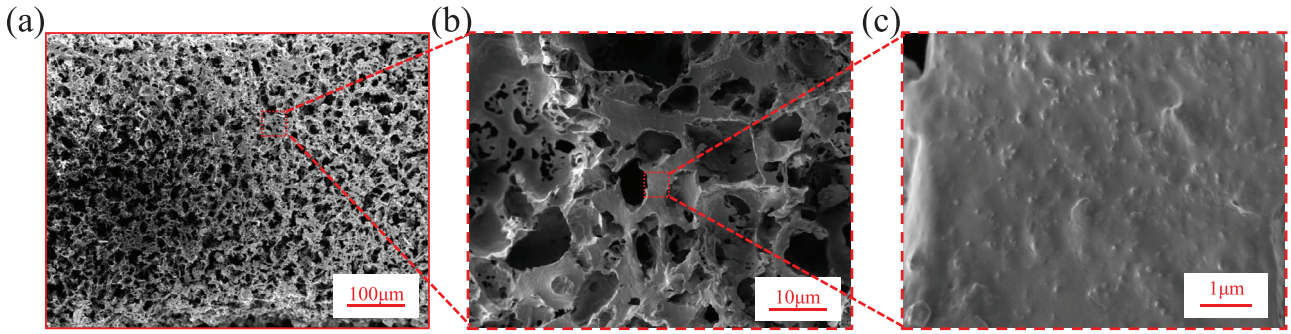

Figure 6. a) Optical images of a microporous material (ACB 15 wt% and porosity 75 v%). b) SEM figures of a compressed microporous material. c) SEM figure of wall of a micropore.

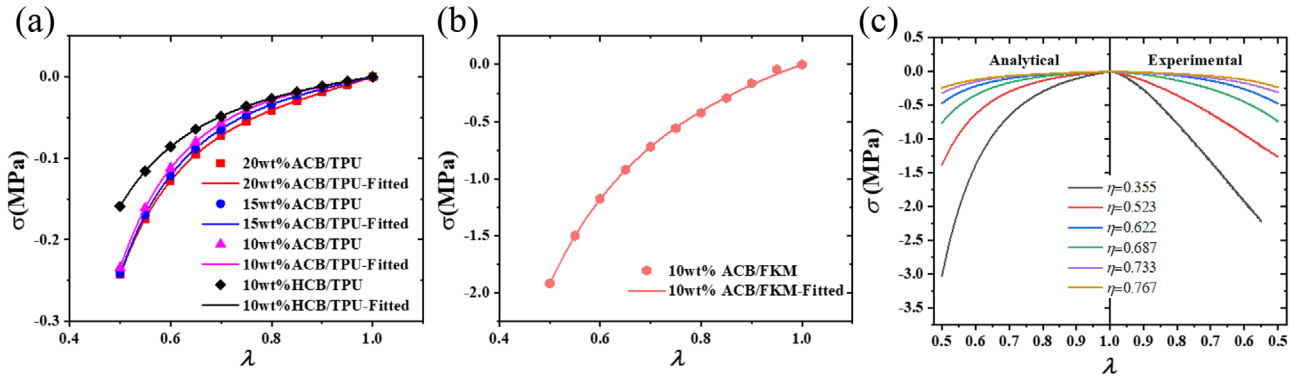

Figure 7. a) Stress-elongation curves of microporous nanocomposite with different contents of ACB (acetylene black) and HCB (highly conductive carbon black). b) Stress-elongation curves of an ACB/FKM microporous nanocomposite. c) Stress-elongation curves of microporous nanocomposites with different porosities.

with *COND* as original conductivity, *FLUX*, *DTEMDS*, *DFDG*, and *NE* as electrical current, the spatial gradients of temperature, the heat flux vector with respect to the spatial gradients of temperature and nominal strain in ABAQUS, respectively. Also, thermal conductance in interaction module was applied to define the ECR with pressure. C3D8T element is chosen to discretize the geometry with the amount of 210,000, which is enough to ensure the results to be convergent and accurate.

Table 1. Key mechanical parameters of microporous nanocomposites.

	μ_1	α_1	μ_2	α_2
10wt%ACB/TPU	0.02689	6.44	0.02713	−2.6769
15wt%ACB/TPU	0.04456	6.65	0.02813	−2.5832
20wt%ACB/TPU	0.07225	6.86	0.02722	−2.4937
10wt%HCB/TPU	0.03535	2.62	0.0152	−2.517
10wt%ACB/FKM	0.6982	1.26	0.0954	−2.23

4. Results and Discussion

Piezoresistive properties, including microstructure, mechanical properties and electrical properties, of the microporous material are studied in the earlier part of the section. A SEM figure of the CB/TPU microporous nanocomposite with 75v% porosity and 15wt% acetylene carbon black (ACB) is shown in **Figure 6**. Figure 6a,b demonstrates the multilevel micropores, which endows the microporous sensor with higher sensitivity than a non-porous sensor. Figure 6c shows conductive CB nanoparticles in the wall of micropores. These CB nanoparticles provide a conductive path and a part of piezoresistive sensitivity.[34]

Then, the mechanical behaviors of the typical microporous nanocomposites are studied based on Equation (7). The influence of the conductive filler including content and kinds on mechanical behaviors is studied with TPU matrix and 75vt% porosity. The result reveals that doping CB nanoparticles is beneficial to strengthen mechanical property. The nanocomposites reinforced by highly conductive carbon black (HCB) with longer chains are softer than those reinforced by ACB. And the effect also occurs in non-porous material systems.[35] Besides, the TPU matrix can be replaced with fluorosilicone rubbers (FKM). **Figure 7**b shows the harder mechanical property of ACB/FKM nanocomposites than that of ACB/TPU, which would reduce sensitivity to pressure. **Table 1** shows the key parameters fitted by the model with the experimental data. Then, taking the fitting parameters of an ACB/TPU nanocomposite (ACB 15 wt% and porosity 75%) as an example, the mechanical behaviors of ACB/TPU nanocomposites with different porosities are predicted. Figure 7c shows the compression with the predicted results and experimental results. These stress–elongation curves show that highly porous nanocomposites($\eta \geq 50\%$) are endowed

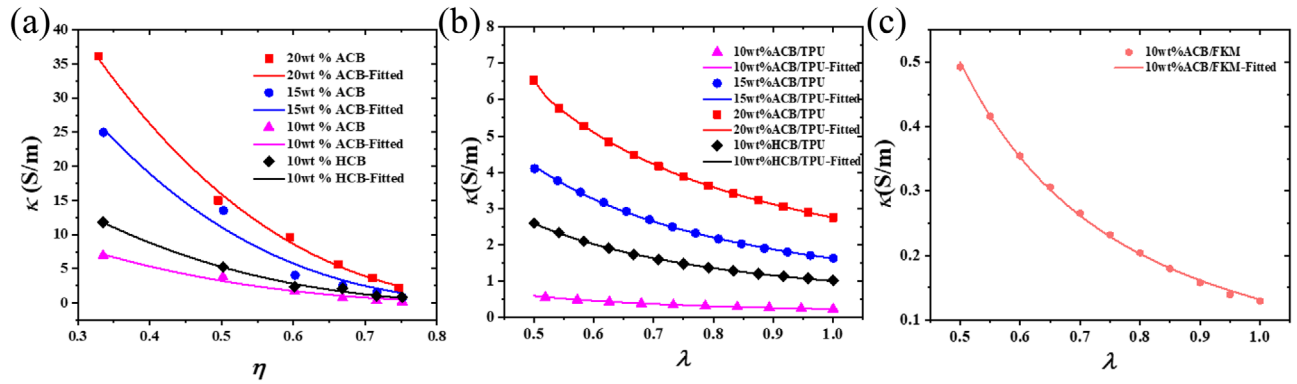

Figure 8. Conductivity–porosity curves (a) and conductivity–elongation curves (b) of microporous nanocomposites with different contents of ACB (acetylene black) and HCB (highly conductive carbon black). c) Conductivity–elongation curves of an ACB/FKM microporous nanocomposite.

with high compressibility to conform to the analytical model, but low porous ones tend to be linear elastic materials.

Based on Equations (8) and (10), the piezoresistive behaviors of the typical microporous nanocomposites are studied. In previous researches of porous medium, the porosity-resistivity relational expressions are summarized and the cementation exponent m is studied.[25] These researches point that the values of m may be higher than 2.5 in high porous medium like the microporous nanocomposite in this study. By adjusting the content of NaCl to change the porosity of the nanocomposite, this deduction about the conductivity–porosity relationship is validated in **Figure 8**a. The values of m are fitted out by Equation (8) and are stabilized at

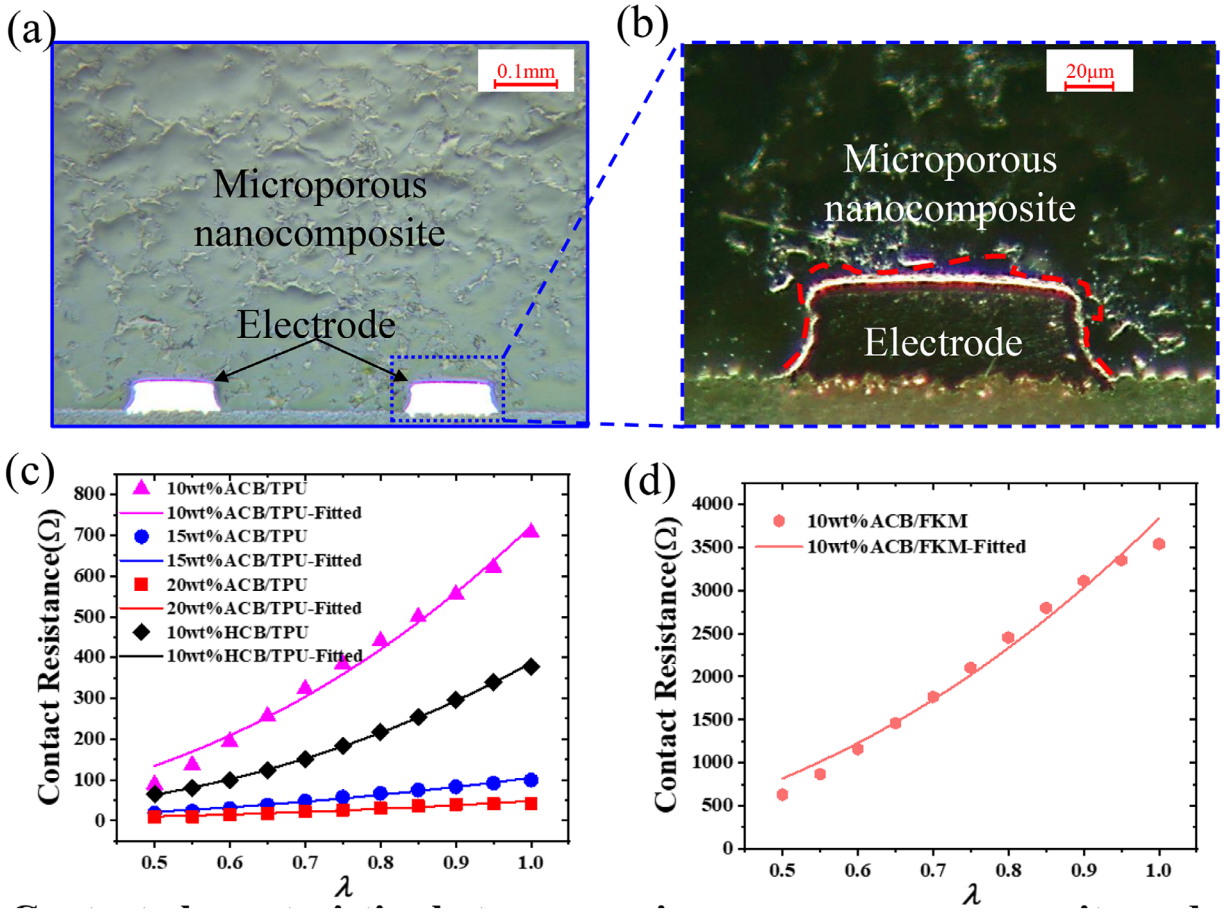

Figure 9. Contact characteristics between a microporous nanocomposite and electrodes. a) Optical cross-sectional view of the contact interface. b) Dark cross-sectional image of the megascopic contact between microporous nanocomposites and electrodes. c) ECR- elongation curves of these microporous nanocomposites with different contents of ACB (acetylene black) and HCB (highly conductive carbon black). d) ECR - elongation curves of an ACB/FKM microporous nanocomposite.

Table 2. Electrical property and ECR parameters of microporous nanocomposites.

	m	a	b	κ_0	A_{ged}
10wt%ACB/TPU	2.77	1.39	1.04	22.0	0.2082
15wt%ACB/TPU	2.93	1.36	0.93	84.7	0.5457
20wt%ACB/TPU	2.75	1.23	1.09	109.3	0.6292
10wt% HCB/TPU	2.82	1.37	1.25	37.2	0.3190
10wt%ACB/FKM	-	1.92	0.31	$0.132/0.25^m$	-

≈2.8 at these nanocomposites with different CB contents and CB types. Then, deformation–conductivity relation of microporous nanocomposites with different fillers and matrix are studied and the quantitative coefficient a is fitted out based on Equation (10). The fitted curves and experimental curves are shown in Figures 8b and 8c. These high fitting degrees($R-Squared \geq 99\%$) show that the modified empirical equation can accurately represent the piezoresistive behaviors of high porous medium. These strain-resistivity quantitative coefficients a are ≈1.3 in CB/TPU systems and ≈1.9 in CB/FKM systems. Increasing CB contents and doping highly conductive CB is of benefit to increase conductivity but has few concerns with the sensitivity to deformation. Replacing TPU matrix with FKM matrix can increase the sensitivity to deformation but may reduce the sensitivity to pressure as shown in Figure 7b.

Before analyzing piezoresistive performance of microporous nanocomposite-based sensors, we need to figure out contact characteristics at the porous interface. The cross-sectional views in **Figure 9**a,b show the contact interface characteristics with the red dotted line representing porous interface of the material. The microstructure of the porous interface demonstrates that the effective conductive areas are far lower than the areas of electrode and ECR is non-negligible. Based on the ECR-deformation relational expression in Equation (13), the contact–strain correlation index b is figured out. The fitted curves with high fitting degrees ($R-Squared \geq 96\%$) are shown in Figure 9c,d. And then the values of b are ≈1.0 in the CB/TPU system and ≈0.3 in the CB/FKM system.

Above all, the electrical behaviors of the microporous nanocomposites are analyzed sufficiently. And these electrical parameters are shown in **Table 2** in detail. m, a, and b are mainly decided by the matrix of the microporous nanocomposite. The content and kind of conductive fillers mainly change conductivity of the microporous nanocomposite and have few contacts with sensitivity to deformation. The FKM matrix can increase the sensitivity to deformation but reduce conductivity and the sensitivity to pressure.

Piezoresistive behaviors of the microporous nanocomposites are studied and intrinsic equations of mechanical property, electrical property, and ECR property are validated in the above paragraph. Taking these piezoresistive parameters of the HCB/TPU nanocomposite (75 v% porosity and 10 wt% HCB) as an example, piezoresistive performances of the microporous nanocomposite-based sensor are further studied based on these intrinsic equations. A simple sensor with a pair of electrodes is studied in terms of an analytical model in Equation (34) confirmed by experiment and FEA. **Figure 10** shows approximate linear resistance–pressure curves and gradually decreasing sensitivity to pressure due to the high compressibility of the microporous nanocomposite. The high consistence between experimental results and analytical results shows the accuracy of analytical prediction. Next, the effect on the performance of the microporous nanocomposite-based sensor is analyzed to guide the design of the sensor based on the analytical model.

Moreover, sensitivity to deformation and sensitivity to pressure at the original state ($\lambda = 1$) as metrics for sensor quality are studied. According to above scaling law model, the influence of size, configuration, effective areas, and porosity on sensitivity is analyzed in this paragraph. **Figure 11** shows the effect of size and configuration on the sensitivity to deformation. The contour in Figure 11a indicates that increasing the distance from electrodes to the border of the sensing layer is of benefit to increase the sensitivity and the contour in Figure 11b shows that increasing the thickness and width of the sensing layer can increase the

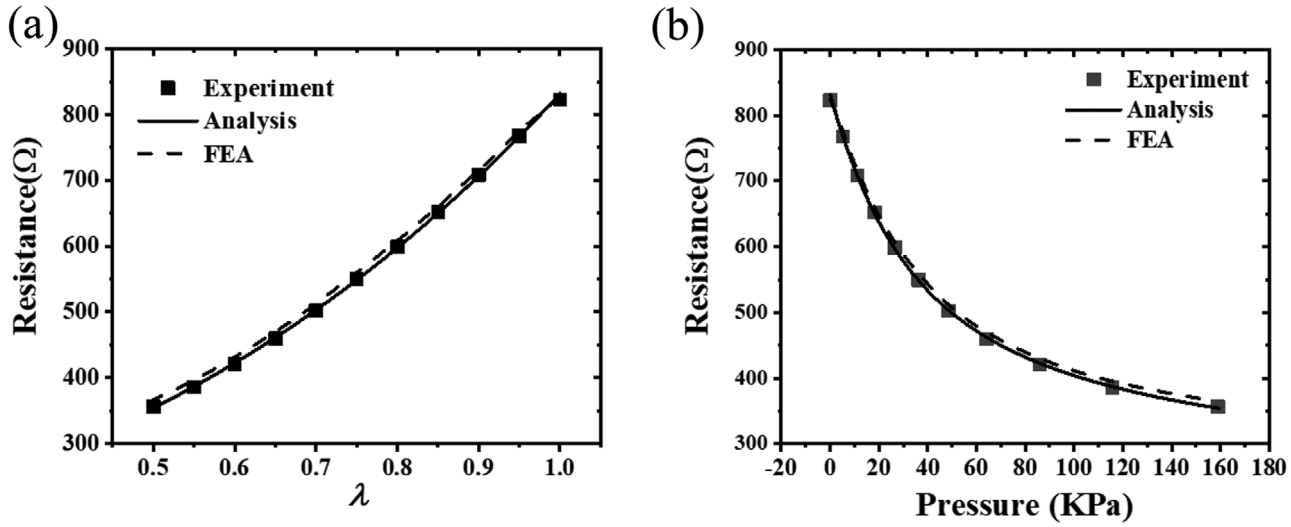

Figure 10. Resistance–elongation (a) and resistance–stress curves (b) from experiment, FEA, and analytical model.

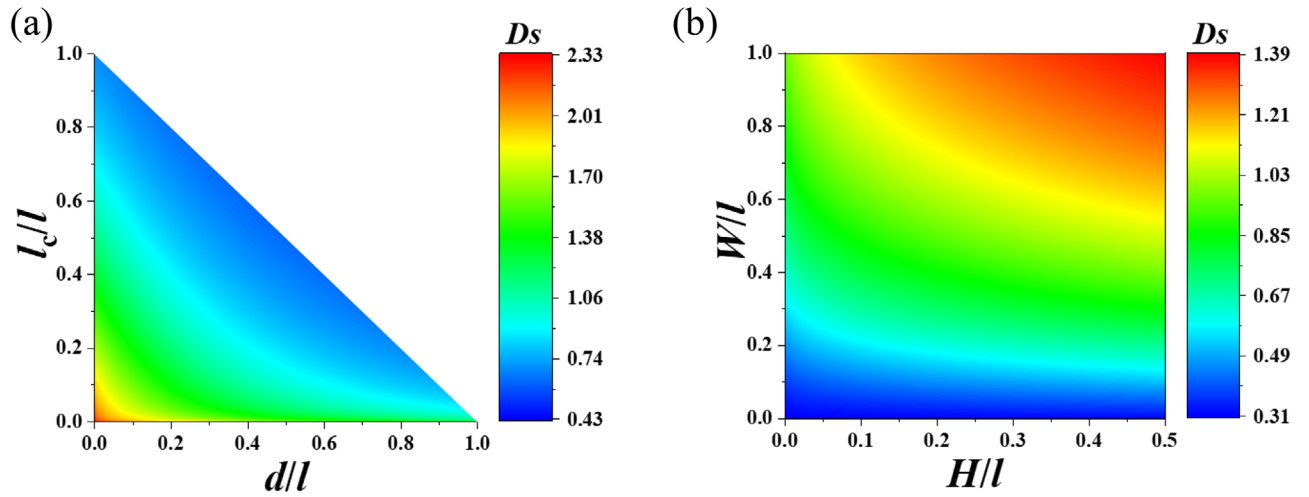

Figure 11. Contour of the maximum sensitivity with respect to elongating influenced by electrode width and distances (a) and sensors' size (b).

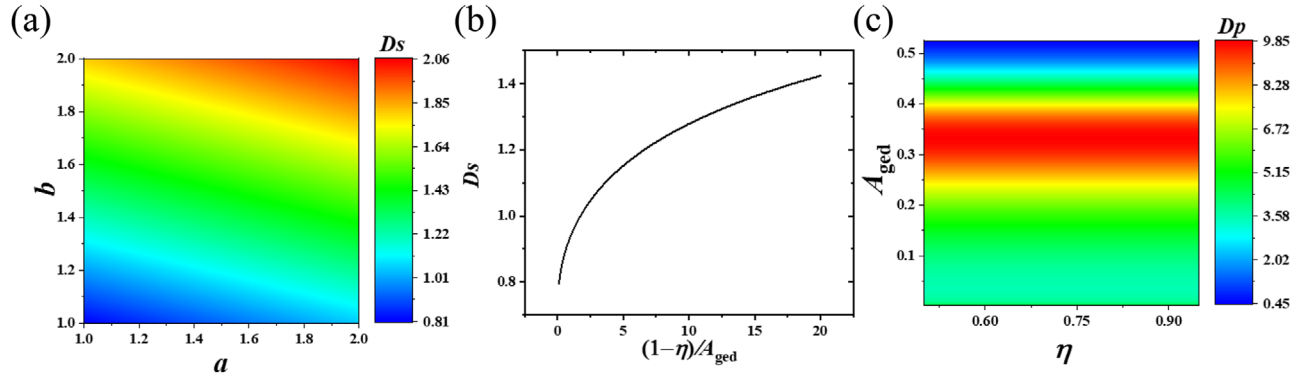

Figure 12. a) Contour of the maximum sensitivity to deformation influenced by quantitative coefficient a and b. b) Maximum sensitivity to deformation changed with scaling parameters $(1-\eta)/A_{ged}$. c) Contour of the maximum sensitivity to pressure influenced by effective areas and porosity.

sensitivity due to the decrease of the original resistance. Then, **Figure 12** illustrates the effect of material property, including porosity η, effective contact area per unit areaA_{ged}, and quantitative coefficient a and b, on the sensitivity. By means of improving the microporous structure, the increase of quantitative coefficient a and b can increase the sensitivity directly because of their linear relation $D_S = a + Db - E$, with D and E as structural parameters. A higher value of $(1-\eta)/A_{ged}$ represents better interfacial condition, which means higher sensitivity as shown in Figure 12b. The sensitivity to pressure is in direct proportion to the sensitivity to deformation. Therefore, above studies are the same with the sensitivity to pressure, except the effect of porosity, which changes the mechanical property. Figure 12c shows the effect of porosity and effective contact area per unit area on the sensitivity to pressure. This contour indicates that the effect of porosity relative to that of the effective area can be ignored.

Finally, piezoresistive behaviors of a sensor integrated with an interdigitated electrode is studied. A typical electrode with ten pairs of interdigital is taken as an example, in Figure 4. The analytical model is established by ignoring transversal conducting traces. The linear superposition of potential at vertical conducting traces is applied to calculate the piezoresistive behavior. **Figure 13**a indicates the accuracy of analytical model by comparing it with the FEA model. The accuracy is beneficial to guide the design of an interdigitated electrode. Keeping the total area of contact region between electrodes and sensing layer, the paired number N of the interdigital electrode is optimized by analyzing its effect on sensitivity. Meanwhile, keeping the size of the sensing layer, the effect of duty (the specific value of contact area against the total area in a single period) on sensitivity is studied. The contour in Figure 13b shows the effect of the number of pairs and duty on sensitivity. Increasing the number of pairs and duty can enhance the sensitivity to deformation and pressure.

5. Conclusion

In order to obtain effective design guidelines for highly compressible sensors made of microporous nanocomposites, we took a microporous CB/TPU system as an example and studied its piezoresistive behavior using an analytical model. Some key parameters of the model were established by experimental results and validated by FEA. When compressing the microporous nanocomposite, the micropores start to close and induce an increase of conductivity and a decrease of ECR, both of which

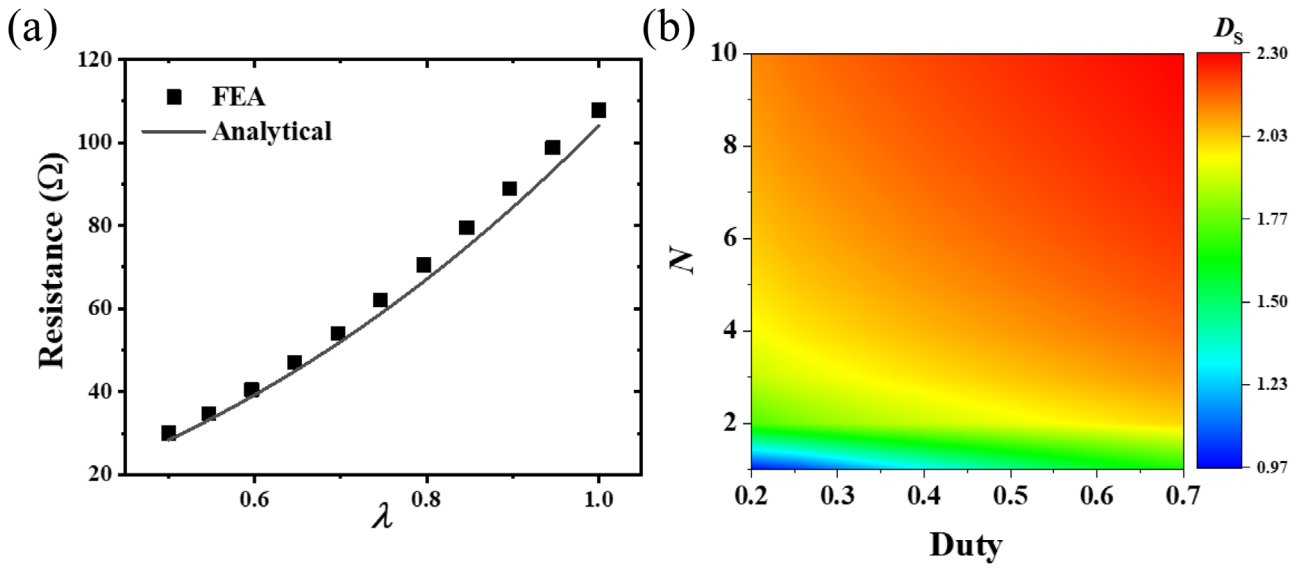

Figure 13. a) Piezoresistive behaviors of the sensor consisting of sensing layers and interdigitated electrodes. b) Effects of the number of pair and duty on sensitivity.

reduce the total resistance and lead to high sensitivity to pressure. We also employed scaling law and the linear superposition principle to systemically analyze the effect of the configuration of the electrodes, the dimension of the sensing layer, and the contact conditions on the sensor performance. Increasing the periphery and the lateral dimension of the sensing layer, the number of electrode pairs, and the effective contact area between the sensing layer and the electrodes can effectively enhance the piezoresistive sensitivity of the microporous nanocomposite-based sensor.

Appendix

ABAQUS UMAT

```
C Defining the field quantity to volumetric strain rate of the element
SUBROUTINE USDFLD(FIELD, STATEV, PNEWDT, DIRECT, T, CELENT, TIME, DTIME, CMNAME, ORNAME, NFIELD, NSTATV, NOEL, NPT, LAYER, KSPT, KSTEP, KINC, NDI, NSHR, COORD, JMAC, JMATYP, MATLAYO, LACCFLA)
C
   INCLUDE "ABA_PARAM.INC"
C
   CHARACTER*80 CMNAME, ORNAME
CHARACTER*3 FLGARY(15)
DIMENSION FIELD(NFIELD), STATEV(NSTATV), DIRECT(3, 3), T(3, 3), TIME(2)
   DIMENSION ARRAY(15), JARRAY(15), JMAC(*), JMATYP(*), COORD(*)
C Obtain the total strain tensor of nodes
CALL GETVRM("NE", ARRAY, JARRAY, FLGRAY, JRCD, JMAC, JMATYP, MATLAYO, LACCFLA)
C Calculate the volumetric strain rate
VEPS = ARRAY(1)+ARRAY(2)+ARRAY(3)
C The volume strain is stored in a state variable and passed to the subroutine UMATHT
STATEV(1) = 1+ARRAY(1)
   STATEV(2) = 1+ARRAY(2)
   STATEV(3) = 1+ARRAY(3)
C
RETURN
END
C Calculate conductivity (the thermal control equation is the same as the electric control equation, and steady-state heat conduction is used instead of electric conduction)
   SUBROUTINE UMATHT(U, DUDT, DUDG, FLUX, DFDT, DFDG, STATEV, TEMP, DTEMP, DTEMDX, TIME, DTIME, PREDEF, DPRED, CMNAME, NTGRD, NSTATV, PROPS, NPROPS, COORDS, PNEWDT, NOEL, NPT, LAYER, KSPT, KSTEP, KINC)
C
   INCLUDE "ABA_PARAM.INC"
C
   CHARACTER*80 CMNAME
   DIMENSION DUDG(NTGRD), FLUX(NTGRD), DFDT(NTGRD), DFDG(NTGRD, NTGRD), STATEV(NSTATV), DTEMDX(NTGRD), TIME(2), PREDEF(1), DPRED(1), PROPS(NPROPS), COORDS(3)
C Defining material properties
C PROPS(1)-Conductivity of the base material
C PROPS(2)-Initial porosity
C PROPS(3)- m value
C STATEV(1)-Volume strain
   COND0 = PROPS(1)
   NF = PROPS(2)
M = PROPS(3)
   B = PROPS(4)
A = PROPS(5)
VPS1 = STATEV(1)
   VPS2 = STATEV(2)
   VPS3 = STATEV(3)
   VP1 = (VPS1**(-A))*((VPS2*VPS3)**(-B))
```

```
   VP2 = (VPS2**(-A))*((VPS1*VPS3)**(-B))
   VP3 = (VPS3**(-A))*((VPS2*VPS1)**(-B))
COND = ((1-NF)**M)*COND0
C Calculate the heat (electricity) conduction matrix
   FLUX(1) = -COND*DTEMDX(1)*VP1
   DFDG(1, 1) = -COND*VP1
   FLUX(2) = -COND*DTEMDX(2)*VP2
   DFDG(2, 2) = -COND*VP2
   FLUX(3) = -COND*DTEMDX(3)*VP3
   DFDG(3, 3) = -COND*VP3
   C DO I = 1, NTGRD
C FLUX(I) = -COND*DTEMDX(I)
C DFDG(I, I) = -COND
C END DO
C
   RETURN
   END
```

Acknowledgements

This work was financially supported by the Science and Technology Innovation Commission of Shenzhen (KQTD20170810105439418, JCYJ20170818091233245, JCYJ20200109114237902).

Conflict of Interest

The authors declare no conflict of interest.

Author Contributions

J.Z.: conceptualization, methodology, formal analysis, finite element analysis, experimental analysis, writing – original draft. Z.W.: experimental guidance, methodology, formal analysis, writing – review and editing. Z.P.: supervision, methodology, funding acquisition, resources, writing – review and editing.

Data Availability Statement

Research data are not shared.

Keywords

finite element analysis (FEA), microporous nanocomposites, multi-mechanism modelling, piezoresistive properties, scaling law

Received: July 9, 2021
Revised: September 15, 2021
Published online:

[1] D. H. Kim, N. S. Lu, R. Ma, Y. S. Kim, R. H. Kim, S. D. Wang, J. Wu, S. M. Won, H. Tao, A. Islam, K. J. Yu, T. I. Kim, R. Chowdhury, M. Ying, L. Z. Xu, M. Li, H. J. Chung, H. Keum, M. McCormick, P. Liu, Y. W. Zhang, F. G. Omenetto, Y. G. Huang, T. Coleman, J. A. Rogers, *Science* **2011**, *333*, 838.
[2] M. L. Hammock, A. Chortos, B. C. K. Tee, J. B. H. Tok, Z. A. Bao, *Adv. Mater.* **2013**, *25*, 5997.
[3] F. Xu, T. J. Lu, K. A. Seffen, *J. Mech. Phys. Solids* **2008**, *56*, 1852.
[4] H.-J. Kim, K. Sim, A. Thukral, C. Yu, *Sci. Adv.* **2017**, *3*, e1701114.
[5] K. Sim, Z. Rao, Z. Zou, F. Ershad, J. Lei, A. Thukral, J. Chen, Q.-A. Huang, J. Xiao, C. Yu, *Sci. Adv.* **2019**, *5*, eaav9653.
[6] S. Wang, J. Xu, W. Wang, G.-J. N. Wang, R. Rastak, F. Molina-Lopez, J. W. Chung, S. Niu, V. R. Feig, J. Lopez, T. Lei, S.-K. Kwon, Y. Kim, A. M. Foudeh, A. Ehrlich, A. Gasperini, Y. Yun, B. Murmann, J. B. H. Tok, Z. Bao, *Nature* **2018**, *555*, 83.
[7] G. Cooper, A. T. Barker, B. W. Heller, T. Good, L. P. J. Kenney, D. Howard, *Med. Eng. Phys.* **2011**, *33*, 967.
[8] P. Chakraborty, T. Guterman, N. Adadi, M. Yadid, T. Brosh, L. Adler-Abramovich, T. Dvir, E. Gazit, *ACS Nano* **2019**, *13*, 163.
[9] M. A. Darabi, A. Khosrozadeh, R. Mbeleck, Y. Q. Liu, Q. Chang, J. Z. Jiang, J. Cai, Q. Wang, G. X. Luo, M. Xing, *Adv. Mater.* **2017**, *29*, 1700533.
[10] R. Kroon, D. A. Mengistie, D. Kiefer, J. Hynynen, J. D. Ryan, L. Y. Yu, C. Muller, *Chem. Soc. Rev.* **2016**, *45*, 6147.
[11] S. Khan, L. Lorenzelli, *Smart Mater. Struct.* **2017**, *26*, 083001.
[12] J. C. Huang, *Adv. Polym. Technol.* **2002**, *21*, 299.
[13] R. Moradi-Dastjerdi, K. Behdinan, B. Safaei, Z. Y. Qin, *Int. J. Mech. Sci.* **2020**, *188*, 105966.
[14] Z. Y. Wang, X. Guan, H. Y. Huang, H. F. Wang, W. E. Lin, Z. C. Peng, *Adv. Funct. Mater.* **2018**, *29*, 1807569.
[15] X. Tang, C. Wu, L. Gan, T. Zhang, T. Zhou, J. Huang, H. Wang, C. Xie, D. Zeng, *Small* **2019**, *15*, 1804559.
[16] X. Wang, Y. Gu, Z. Xiong, Z. Cui, T. Zhang, *Adv. Mater.* **2014**, *26*, 1336.
[17] X. Guan, Z. Y. Wang, W. Y. Zhao, H. Y. Huang, S. P. Wang, Q. Zhang, D. X. Zhong, W. N. Lin, N. Ding, Z. C. Peng, *ACS Appl. Mater. Interfaces* **2020**, *12*, 26137.
[18] Z. R. Wang, S. Wang, J. F. Zeng, X. C. Ren, A. J. Y. Chee, B. Y. S. Yiu, W. C. Chung, Y. Yang, A. C. H. Yu, R. C. Roberts, A. C. O. Tsang, K. W. Chow, P. K. L. Chan, *Small* **2016**, *12*, 3827.
[19] S. Meskinis, R. Gudaitis, A. Vasiliauskas, A. Ciegis, K. Slapikas, T. Tamulevicius, M. Andrulevicius, S. Tamulevicius, *Diamond Relat. Mater.* **2015**, *60*, 20.
[20] A. A. Barlian, W. T. Park, J. R. Mallon, A. J. Rastegar, B. L. Pruitt, *Proc. IEEE* **2009**, *97*, 513.
[21] C. Zhang, W. B. Ye, K. Zhou, H. Y. Chen, J. Q. Yang, G. L. Ding, X. L. Chen, Y. Zhou, L. Zhou, F. J. Li, S. T. Han, *Adv. Funct. Mater.* **2019**, *29*, 1808783.
[22] Y. Shindo, Y. Kuronuma, T. Takeda, F. Narita, S. Y. Fu, *Composites, Part B* **2012**, *43*, 39.
[23] D. D. L. Chung, *J. Mater. Sci.* **2020**, *55*, 15367.
[24] B. Storåkers, *J. Mech. Phys. Solids* **1986**, *34*, 125.
[25] J. C. Cai, W. Wei, X. Y. Hu, D. A. Wood, *Earth-Sci. Rev.* **2017**, *171*, 419.
[26] N. Khalili, H. E. Naguib, R. H. Kwon, *Soft Matter* **2016**, *12*, 4180.
[27] Y. Cui, Z. G. Bian, Y. H. Li, Y. F. Xing, J. Z. Song, *J. Phys. D: Appl. Phys.* **2016**, *49*, 405101.
[28] B. Fazekas, T. J. Goda, *Mater. Des.* **2018**, *156*, 596.
[29] P. Steinmann, M. Hossain, G. Possart, *Arch. Appl. Mech.* **2012**, *82*, 1183.
[30] M. Hossain, A. F. M. S. Amin, M. N. Kabir, *J. Mech. Behav. Mater.* **2015**, *24*, 11.
[31] *Abaqus, Dassault Systèmes, Simulia Corporation*, Providence, Rhode Island **2016**.
[32] S. Thelen, F. Barthelat, L. C. Brinson, *J. Biomed. Mater. Res., Part A* **2004**, *69A*, 601.
[33] G. E. Archie, *Trans. AIME* **1942**, *146*, 54.
[34] M. Hussain, Y. H. Choa, K. Niihara, *Composites, Part A* **2001**, *32*, 1689.
[35] N. Rattanasom, T. Saowapark, C. Deeprasertkul, *Polym. Test.* **2007**, *26*, 369.